Journal of Applied Electrochemistry **34**: 1235–1240, 2004.

Flow influenced electrochemical corrosion of nickel aluminium bronze – Part I. Cathodic polarisation

G. KEAR[1,*], B.D. BARKER[2], K. STOKES[3] and F.C. WALSH[4]
[1]*Building Research Association of New Zealand (BRANZ) Ltd., Private Bag 50 908, Porirua City 6220, New Zealand*
[2]*Applied Electrochemistry Group, Centre for Chemistry, University of Portsmouth PO1 2DT, UK*
[3]*DSTL Winfrith, Winfrith Technology Park, Dorchester, DT2 8WX, UK*
[4]*Electrochemical Engineering Group, School of Engineering Sciences, University of Southampton, Highfield SO17 1BJ, UK (*author for correspondence, e-mail: Gareth Kear@branz.co.nz)*

Received 12 November 2003; accepted in revised form 14 July 2004

Key words: flow-enhanced corrosion, mass transfer, nickel aluminium bronze (NAB), oxygen reduction, rotating cylinder electrode (RCE), rotating disc electrode (RDE), seawater

Abstract

The cathodic polarisation behaviour of CA 104 nickel aluminium bronze (NAB) has been examined in fully characterised seawaters (filtered and artificial) using the rotating disc electrode (RDE) and the rotating cylinder electrode (RCE). Linear sweep voltammetry and a potential step, current transient technique were used to examine the charge transfer and mass transfer controlled cathodic response as a function of both laminar and turbulent fluid flow. For freshly polished surfaces, the rate of irreversible charge transfer controlled oxygen reduction is controlled by the exchange of a single electron and hydrogen evolution is only significant at potentials more negative than approximately −1.0 V vs. the saturated calomel electrode (SCE).

1. Introduction

The NAB alloys have a long history of acceptable resistance to marine cavitation and flow-enhanced corrosion [1, 2]. NAB materials have been extensively used for ship propeller material and marine heat exchanger/condenser systems [3, 4]. The alloys are also used in the manufacture of values, tube plates, strainer bodies and pump castings, shafts and impellers [2, 4–9]. The materials can suffer surface damage, however, under conditions of extreme flow velocity or fluid disturbance. The common commercial alloys, which both contain about 10% aluminium, 5% nickel and 5% iron, are BS 2874 CA 104 (for wrought alloys) and BS 1400 (for cast alloys). The composition of the alloy used in this work (CA 104) is given in Table 1.

Unlike materials such as unalloyed copper and the copper–nickels, the NAB have received very little attention to their interfacial and electrochemical behaviour in aqueous chloride media. In the case of copper, oxygen reduction and the chloride ion facilitated dissolution dominate the cathodic and anodic reactions, respectively [10]. In the only kinetic study of NAB corrosion in aqueous chloride environments, Schussler and Exner [11, 12] examined the behaviour of cast NAB in synthetic seawaters using only a single fluid velocity. Linear Tafel kinetics with cathodic slope of −0.140 V decade^{-1} were observed for freshly polished surfaces and the number of electrons exchanged in the cathodic reaction was assumed to be 1.

The elucidation of the mass transfer effects influencing NAB behaviour in seawater is extremely important if the previously unexamined electrochemical corrosion mechanism is to be determined. Quantitative analysis of both the charge and mass transfer controlled components of the cathodic and anodic polarisation characteristics within single phase, laminar and turbulent fluid flow is possible through the use of the established RDE [13–16] and RCE [17–19] geometries. It has been proposed repeatedly that Reynolds number (Re) can be used in conjunction with the principle of equality of mass transfer coefficient (k_m) [20, 21] in the translation of laboratory work to well defined geometries in the field via dimensionless numbers [13, 22–26].

Taking the RDE as an example, k_m can be described as a function of limiting current density (j_L) diffusion coefficient (D) and thickness of the Nernst diffusion boundary layer (δ_N) close to the electrode surface [13]:

$$k_m = \frac{j_L}{zFc_b} = \frac{D}{\delta_N} = 0.62D^{0.667}\nu^{-0.167}\omega^{0.5} \quad (1)$$

z, F and c_b are the stoichiometric number of electrons exchanged in the mass transfer limited reaction, the

Table 1. Alloy percentage elemental composition (wt/wt) conforming to BS 2874: 1986: CA 104 (suppliers analysis)

Cu	Fe	Si	Mn	Pb	Al	Ni	Mg	Zn
Bal.	4.43	0.05	0.14	0.02	9.31	4.65	0.01 max.	0.11

Faraday constant and the bulk or interfacial concentration of the electroactive species. The kinematic viscosity of the fluid and the electrode angular velocity are represented by ν and ω, respectively. The Levich equation for the smooth RDE in laminar flow (Equation 2) [13] enables a description of a fully mass transfer controlled, current density response as a function of electrode angular velocity:

$$j_{(\mathrm{RDE})} = 0.62zFD^{0.66}\nu^{-0.166}c_{\mathrm{b}}\omega^{0.50} \quad (2)$$

An equivalent expression for a smooth RCE in turbulent flow can also be produced from components of Equation 1 and dimensionless analysis:

$$j_{(\mathrm{RCE})} = 0.085zFD^{0.644}r^{-0.30}\nu^{-0.344}c_{\mathrm{b}}\omega^{0.70} \quad (3)$$

2. Experimental procedure

2.1. *Working electrodes*

Wrought NAB material was supplied by Stone Manganese Ltd. (UK) in rod form to meet BS 2874: 1986: CA 104 (see Table 1). Both the RDE and RCE were designed for use with a Pine Instruments Company, model AFMSRX analytical rotator fitted with the MSRX Arbor–ACMDI1906C rotator arm (1/4 UNF connecting thread). The dimensions of the active section of the RDE were diameter 0.401 cm and area 0.126 cm^2. The active section of the RCE consisted of diameter 1.998 cm, length 1.602 cm and area 10.06 cm^2. High-density polyethylene rod was used as inert insulating sheathing.

The working electrode surfaces were mechanically polished (manually) on micro-polishing cloth and degreased in ethanol prior to each polarisation and corrosion potential measurement. Mechanical polishing of pre-conditioned electrodes (0.3 μm finish) consisted of a double, 3-min polish with a 0.3 μm α-alumina/distilled water slurry.

Table 2. Total chloride concentration and bicarbonate alkalinity

Source	Bicarbonate alkalinity/ mol dm^{-3}	$[Cl^-]$/mol dm^{-3}
Filtered – Directly measured	0.0027 ± 0.0010	0.550 ± 0.013
Artificial – Directly measured	0.0024 ± 0.0004	0.500 ± 0.013
Literature (seawater at 35% and 25 °C)	0.0024	0.558–0.559
Literature (*via* BS 3900:Part F4:1968)	0.0024	0.543

2.2. *Electrolytes*

Natural seawater was collected from a short-term holding tank at the University of Portsmouth Institute of Marine Sciences (Langstone Harbour, Hampshire, UK). The seawater was subsequently vacuum-filtered down to a 0.2 μm pore size membrane to remove suspended solids, microorganisms and the majority of biological spores. The electrolytic conductivity (κ) of the filtered seawater was adjusted to 50.8 ± 0.1 mS cm^{-1} at 25 ± 0.2 °C using a Metler-Toledo MPC 227 conductivity/pH meter. This value of κ was taken from a long-term study of Langstone Harbour seawater (corrected to 25 °C) [27]. The filtered and conductivity-adjusted seawater (pH 8.05 ± 0.15) was stored in the absence of light at 3 °C. Conductivity adjustment of the filtered seawater ensured that all physical parameters and chemical composition of the seawater remained constant throughout the period of the investigation [28, 29].

Artificial seawater to BS 3900:Part F4:1968 (supplied by BDH) was used as a standard solution for comparison with the filtered seawater. The mean experimental and literature values of the physicochemical quantities of both seawaters, including chloride ion concentration, salinity and dissolved O_2, are given in Tables 2, 3 and 4.

Directly measured values of bicarbonate alkalinity and chloride ion concentration were estimated via

Table 3. Physical parameters of the electrolytes at 25 ± 0.2 °C (literature values for the filtered seawater were calculated assuming conductivity, κ = 50.8 mS cm^{-1})

Source	pH	κ/mS cm^{-1}	S/% (g kg^{-1})	Relative density	ν ($\times 10^2$)/cm^2 s^{-1}
Filtered – Directly measured	8.0 ± 0.2	50.8 ± 0.2	33.4 ± 0.2[(a)(c)] 34.4 ± 0.9[(b)]	1.03 ± 0.01	1.07 ± 0.01
Artificial – Directly measured	7.9 ± 0.1	46.2 ± 1.3	29.8 ± 0.2[(a)(c)] 31.5 ± 0.8[(b)]	1.03 ± 0.01	1.07 ± 0.01
Filtered – Literature	7.9 ± 0.5	–	–	1.03 ± 0.01	0.93 ± 0.01
Artificial – Literature	–	–	–	–	–

Salinity was measured using a Profi-Line LF 197, a WTW Measurement Systems Inc. saliniometer[(a)] via conductivity [28] measurements[(b)] and potentiometric titration [30] against $AgNO_3$[(c)].

Table 4. Values of dissolved oxygen concentration at 25 ± 0.2 °C

Source	Concentration	
	ppm	mol dm^{-3} ($\times 10^4$)
Filtered – Directly measured	6.90 ± 0.30	2.16 ± 0.01
Artificial – Directly measured	7.00 ± 0.30	2.19 ± 0.01
Literature (for κ = 50.8 ± 0.1 mS cm^{-1})	6.80[(a)] 6.66[(b)]	2.13[(a)] 2.08[(b)]

Literature values calculated using the Weiss[(a)] [29] or the Truesdale[(b)] et al. [33] relationships

potentiometric titration [30]. Mean literature values of these parameters along with pH are taken from a general review of tabulated data [2, 29, 31, 32]. Literature concentrations are converted from g kg^{-1} through a standard seawater density at 25 °C of 1.0234 g cm^{-3} [29]. Kinematic viscosity was determined with a B-type Ostwald/U-tube viscometer and dissolved O_2 concentrations were estimated with a Jenway 3420 dissolved oxygen meter. Literature values of O_2 concentration were also calculated using both the Weiss relationship and the Truesdale et al. relationship [29, 33] assuming that when κ=50.8 mS cm^{-1} the salinity (S)=33.4 ± 0.1%. The literature values of relative density and kinematic viscosity were calculated from tabulated data [28].

2.3. *General procedure*

All electrochemical measurements were made at 25 ± 0.2 °C with an Eco hemie Autolab potentiostat (PGSTAT20 computer controlled) using the General Purpose, Electrochemical Software (GPES) version 4.5. The electrochemical cell incorporated a thermostatically controlled, glass water jacket, a platinum gauze counter electrode and a Radiometer Analytical A/S, REF 401, SCE used in conjunction with either a RDE or RCE adapted Luggin-Haber capillary. The RCE radius/cell wall radius gap ratio of 0.33 was predicted to inhibit the formation of Taylor–Couette flow [34, 35].

The electrolyte was aerated for 10 min prior to the commencement of measurements. When necessary, deoxygenation was achieved by purging with 4.0 spot (99.99%) nitrogen (supplied by British Oxygen Company) for 10 min followed by a constant nitrogen blanket above the electrolyte to prevent air ingress. The range of Reynolds numbers for each geometry was Re_{RDE}=79 to 3700 (corresponding to 200–9500 rpm or 29–995 rad s^{-1}) and Re_{RCE}=1900 to 76860 (100–4000 rpm or 10–419 rad s^{-1}).

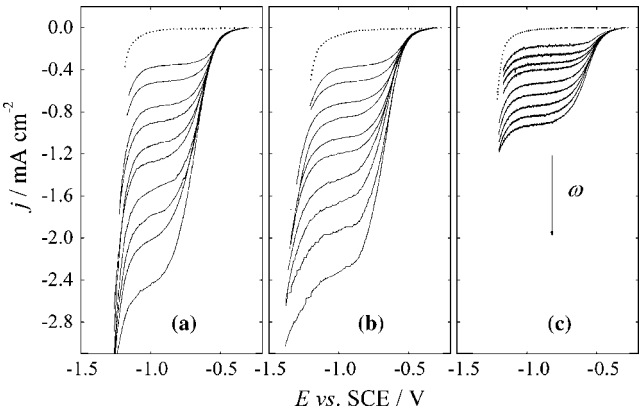

Fig 1. Linear sweep voltammetry describing oxygen reduction at NAB as a function of electrode angular velocity. (a) RDE-artificial seawater, (b) RDE-filtered seawater, and (c) RCE-filtered seawater. Re_{RDE}=79–3740 (21–995 rad s^{-1}); Re_{RCE}=1930–26,900 (10–146 rad s^{-1}). Broken lines indicate currents measured in de-oxygenated electrolytes.

3. Results and discussion

Cathodic linear sweep voltammetry (LSV) at both electrode types and seawaters (Figure 1) revealed a reduction process dominated by a single wave for oxygen reduction:

$$O_2 + 2H_2O + 4e^- \rightarrow 4OH^- \quad (4)$$

No significant production or build up of hydrogen peroxide was observed. The somewhat irreversible initial potential region of charge transfer controlled O_2 reduction lead to values of limiting current density, which showed definite dependency on electrode angular velocity. For Re_{RDE} 79–3700, the range of j_L values was −0.4 to −2.5 mA cm^{-2}. For Re_{RCE} 1900–76900 the equivalent currents were −0.2 to −0.9 mA cm^{-2}. The nature of the laminar flow regime at the RDE, where the fluid is drawn onto the electrode surface in a direction normal to the electrode [13], produces significantly smaller values of δ_N For example, at Re=2000, δ_N^{RDE}=9 μm and δ_N^{RCE}=125 μm. This produces correspondingly higher rates of mass transfer coefficient relative to the RCE for equivalent Reynolds numbers (see Equation 6).

Diffusion coefficients for oxygen (D_{O_2}) at 25 ± 0.2 °C (Table 5) were calculated from experimental

Table 5. Linear regression and diffusion coefficient data taken from Levich slopes for pure oxygen reduction at the NAB-RDE. LSV (linear sweep voltammetry) and PSCT (potential step current transient) indicate method of limiting current measurement

Electrolyte	Measurement technique	Slope ($\times 10^6$)/A $rad^{-0.5}$ $s^{0.5}$	D_{O_2} ($\times 10^5$)/cm^2 s^{-1}	Y intercept ($\times 10^6$)/A	Correlation coefficient
Filtered	LSV	−8.950 ± 0.068	1.65 ± 0.05	1.270 ± 0.070	−0.99993
Seawater	PSCT	−9.020 ± 0.0380	1.67 ± 0.05	−1.670 ± 0.060	−0.99992
Artificial	LSV	−9.610 ± 0.800	1.79 ± 0.05	−1.470 ± 0.010	−0.99972
Seawater	PSCT	−9.760 ± 0.440	1.78 ± 0.05	−1.180 ± 0.060	−0.99996

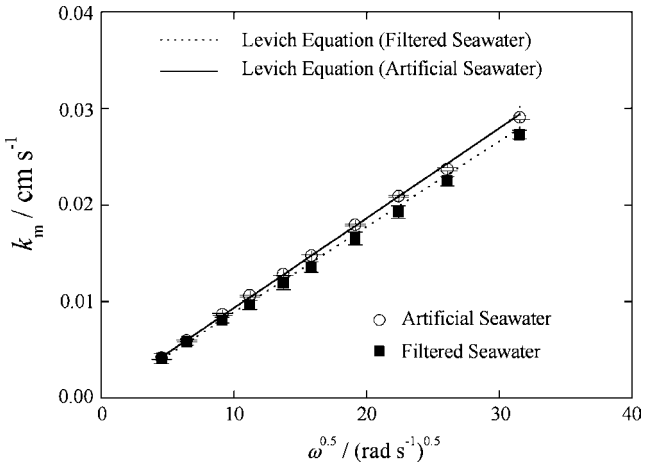

Fig. 2. Plots describing the dependence of the mass transfer coefficient for oxygen as a function of the square root of RDE angular velocity. Lines indicate theoretical current calculated using Equation 2.

RDE Levich slopes (j_L vs. $\omega^{0.5}$) using Equation 2. The overall, mean experimental value of $(1.7 \pm 0.1) \times 10^{-5}$ cm^2 s^{-1} compares well with a seawater and dilute aqueous NaCl literature reviewed mean (corrected to 25 °C) of $(1.9 \pm 0.2) \times 10^{-5}$ cm^2 s^{-1} [25].

Mass transfer coefficients for oxygen were also calculated from j_L values using Equation 1. A typical set of plots calculated from RDE-LSV data are shown in Figure 2 where calculated values of k_m ranged from 0.004 to 0.029 cm s^{-1}. The regression data showed excellent linearity throughout and passed directly through the origin indicating full mass transfer control over O_2 reduction as described by Equation 2.

The cathodic polarisation behaviour of the metals in the mixed charge and mass transfer controlled current region (approximately −0.800 to −0.525 V vs. SCE) was investigated using a potential step, current transient technique with hydrodynamic (rotation rate) steps. Typical trends in E and ω used to study O_2 reduction in the potential region of mixed controlled cathodic current are represented, schematically, in Figure 3. An initial potential was applied and ω was varied in increments (the time scale of which was adjusted to ensure a steady state current response). The rotation rate was then lowered to the original level and, simultaneously; the potential was stepped to a more negative value. The sequence was repeated over the whole range of required overpotentials.

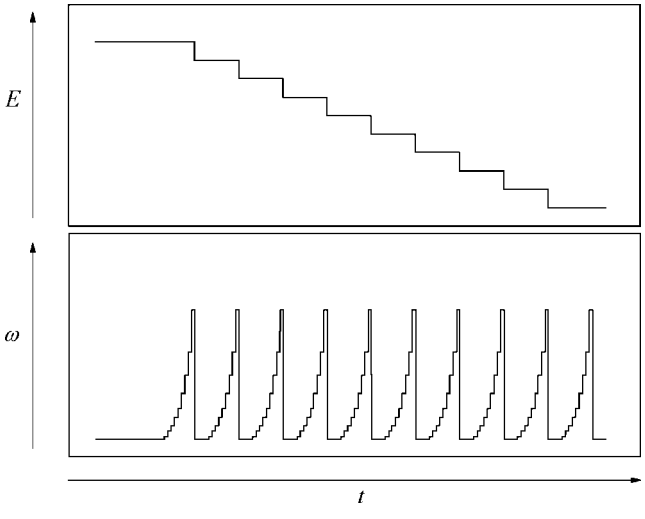

Fig. 3. Schematic applied potential and electrode angular velocity vs. time stimulus response transients, describing the conditions of the multiple overpotential, potential step, current transient procedure.

The Koutecky–Levich approach [36] to the analysis of mixed charge and mass transfer controlled data can be used to accurately extract a current response which is independent of species transport within the electrolyte phase. For the RDE:

$$\frac{1}{j} = \frac{1}{zFkc_b} + \frac{1}{0.62zFc_b v^{-0.167}} \cdot \frac{1}{\omega^{0.5}} \tag{5}$$

where, k is the potential dependent rate constant for the reaction of interest. A typical series of Koutecky–Levich plots are given in Figure 4 for pure O_2 reduction in the artificial seawater. Slopes for both the RDE and the RCE and the filtered and the artificial electrolytes were plotted at equal increments in polarisation of −20 or −25 mV throughout the region of mixed controlled current response. The linear plots show a clear dependence of the current on fluid velocity and the gradients of the slopes are constant with increasing cathodic polarisation. The latter feature indicates an irreversible half-cell reaction [37].

Tafel slopes (β_C) for pure charge transfer controlled O_2 reduction were extracted from the intercepts of the Koutecky–Levich plots on the vertical axis (Figure 5). The linear regression data for the slopes are given in Table 6. Cathodic Tafel slopes can be described by:

$$\beta_C = -\frac{\alpha_C zF}{2.3RT} \tag{6}$$

where, α_C, R and T are the cathodic charge transfer coefficient, the molar gas constant and absolute temperature,

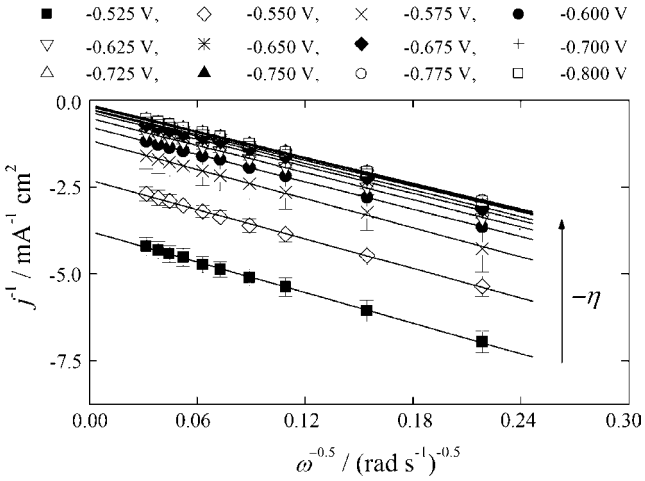

Fig. 4. Koutecky–Levich plots for pure O_2 reduction at the NAB-RDE in the artificial seawater.

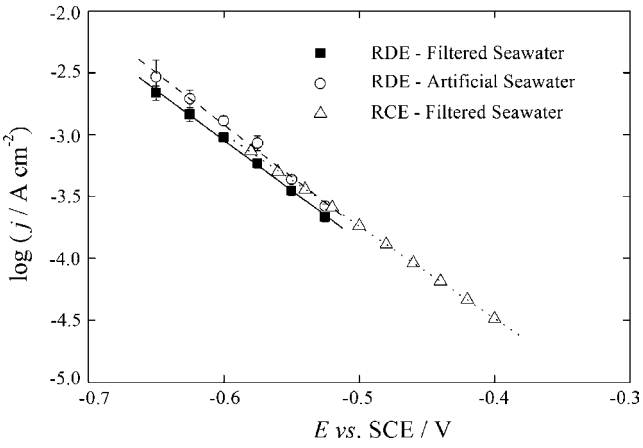

Fig. 5. Comparison of Koutecky–Levich equation derived, Tafel slopes for pure O_2 reduction at rotating NAB electrodes.

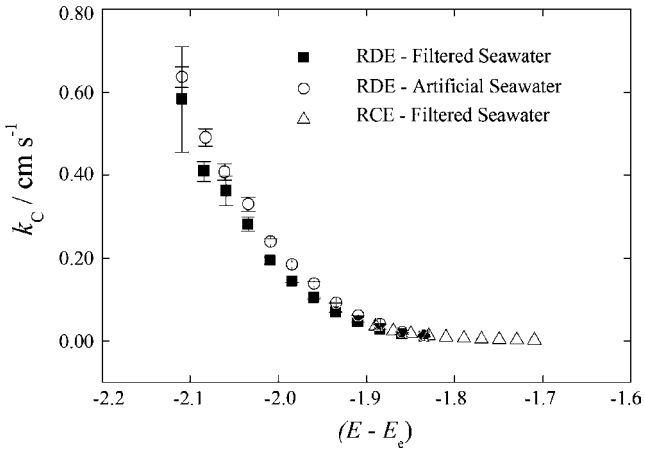

Fig. 6. Potential dependent rate constant for pure O_2 reduction at NAB as a function of $(E - E_e)$. Where $E_e = +1.31$ V vs. SCE under the experimental conditions of this work.

respectively. Taking α_C to equal 0.5, slopes of -0.124 ± 0.003 (RDE-filtered seawater), -0.119 ± 0.005 (RDE-artificial seawater) and -0.149 ± 0.006 V decade^{-1} (RCE-filtered) broadly indicate a limiting step determined by a single electron exchange. This is in agreement with King, et al. [38] for O_2 reduction at pure copper in 1.0 mol dm^{-3} NaCl (23 ± 2 °C) Literature values of the Tafel slope for O_2 reduction at copper vary, depending on the surface condition, electrolyte type, temperature and O_2 concentration and can range from −0.100 [39] and −0.150 V decade^{-1} [38,40] to approximately −0.300 V decade^{-1} [41].

The potential dependent, cathodic rate constant (k_C) for pure O_2 reduction was calculated as a function of overpotential (Figure 6) using the relationship given in Equation 7. The order of reaction with respect to O_2 was taken as 1 [38] and a single electron exchange was assumed.

$$k_C = \frac{j}{zF[O_2]} \tag{7}$$

Resulting values of k_C ranged from 0.002 cm s^{-1} to 0.600 cm s^{-1} over an overpotential range of approximately −1.7 to −2.1 V. The rate of O_2 reduction at NAB appeared to show little variation with changes in electrode geometry or electrolyte. As predicted from Equation 8, where E_e is the reaction equilibrium potential and k_0 is the potential independent electrochemical rate constant, k_C increased exponentially as a function of applied potential.

$$k_C = k_o \exp^{\frac{-zF}{RT}(E-E_e)} = k_o \exp^{B(E-E_e)} \tag{8}$$

Experimental constants relating to Equation 8 are compared in Table 7, where differences in the values of k_o and B between the RDE and RCE geometries are evident but relatively insignificant. This was also the case even at the values of polarisation experienced at the stabilised corrosion potential (≅ −0.295 to −0.330 V vs. SCE).

Overall, the cathodic polarisation behaviour of CA 104 NAB is broadly analogous to that of freshly polished copper in seawater and other aqueous dilute chloride media [10]. Irreversible oxygen reduction is the primary electrochemical reaction close to the corrosion potential and hydrogen evolution is only significant at very large negative values of polarisation from the corrosion potential (≅ −0.7 to −0.8 V).

As expected, difference in the charge transfer behaviour of oxygen reduction is minimal between each of the RDE and RCE flow geometries. Thus, this work has demonstrated the applicability of using of both laminar and turbulent fluid regimes to extract charge transfer controlled data from a mixed mass and charge transfer influenced current response.

Table 6. Linear regression data describing the Tafel slopes for pure oxygen reduction at the NAB-RDE and RCE (see Figure 5)

Source	Tafel Slope/ V decade^{-1} (V/[log{A cm^{-2}}])	Y intercept (Log[A cm^{-2}])	Correlation coefficient
RDE – Filtered seawater	−0.124 ± 0.003	−7.964 ± 0.243	−0.99524
RDE – Artificial seawater	−0.119 ± 0.005	−7.962 ± 0.243	−0.99524
RCE – Filtered seawater	−0.149 ± 0.006	−7.166 ± 0.046	−0.99987

4. Conclusions

1. The cathodic response of NAB in filtered and artificial seawaters has been examined under conditions of controlled laminar and turbulent flow in a highly quantitative manner using both linear sweep voltammetry and a potential step technique.
2. The polarisation behaviour of freshly polished BS CA 104 NAB in dilute chloride media closely emulates that of pure, unalloyed copper where irreversible

Table 7. Experimental constants relating to Equation 8 describing the exponential change in the potential dependent rate constant for pure oxygen reduction as a function of applied potential

Source	E vs. SCE/V	$(E - E_c)$/V	k_o/cm s^{-1}	B
RDE – Filtered seawater	−0.650 to −0.525	−1.960 to −1.834	2.0×10^{-17}	−18.626
RDE – Artificial seawater	−0.650 to −0.525	−1.960 to −1.834	5×10^{-18}	−19.342
RCE – Filtered seawater	−0.580 to −0.400	−1.890 to −1.710	3.00×10^{-16}	−17.182

reduction of oxygen dominates the cathodic process at applied potentials more positive than approximately −1.0 V vs. SCE.

3. Potential dependent, rate constants for oxygen reduction in both the filtered and artificial seawaters ranged from 0.002 to 0.600 cm s^{-1} over a negative polarisation range of approximately −0.1 to −0.7 V.
4. An overall mean diffusion coefficient for oxygen in both electrolytes was determined as $(1.7 \pm 0.1) \times 10^{-5}$ cm^2 s^{-1}.

Acknowledgements

The authors are grateful to DSTL-Farnborough, UK and QinetQ-Haslar, UK for financial contributions to the research programme.

References

1. A. Al-Hashem, P.G. Caceres, W.T. Riad and H.M. Shalaby, *Corrosion* **51** (1995) 331.
2. T.H. Rogers, 'Marine Corrosion' (George Newnes Ltd., London, 1968).
3. R.F. Schmidt and F.L. Riddell, *American Foundary Soc. Trans.* **73** (1965) 471.
4. T.J. Glover, *Mater. Perform.* **27** (1988) 51.
5. F.L. LaQue, 'Marine Corrosion: Causes and Prevention' (John Wiley & Sons, London, 1975).
6. A Working Party Report, European Federation of Corrosion Publications No. 5, 'Illustrated Case Histories of Marine Corrosion', Technical Report (The Institute of Metals, London, 1990).
7. B. Todd and P.A. Lovett, 'Marine Engineering Practice: Selecting Materials for Sea Water Systems', Technical Report (The Institute of Marine Engineers, London, 1974).
8. A.H. Tuthill, *Mater. Perform.* **26** (1987) 12.
9. L. Kenworthy, *Trans. Inst. Marine Eng.* **77** (1965) 149.
10. G. Kear, D.B. Barker and F.C. Walsh, *Corros. Sci.* **46** (2004) 109.
11. A. Schussler and H.E. Exner, *Corros. Sci.* **34** (1993) 1793.
12. A. Schussler and H.E. Exner, *Corros. Sci.* **34** (1993) 1803.
13. V.G. Levich, 'Physicochemical Hydrodynamics' (Prentice-Hall Inc., Englewood Cliffs, New Jersey, 1962).
14. G. Kear, F.C. Walsh, D.B. Barker and K.S. Stokes, 'Electrochemical Corrosion Characteristics of Copper in Filtered and Artificial Seawater as a Function of Mass Transfer Conditions', proceedings of EuroCorr 2000, Queen Mary and Westfield College, University of London, Institute of Corrosion, 10–14 September 2000.
15. S.R. de Sanchez and D.J. Schiffrin, *Corros. Sci.* **22** (1982) 585.
16. F. King, C.D. Litke, M.J. Quin and D.M. LeNeveu, *Corros. Sci.* **37** (1995) 833.
17. D.R. Gabe, *J. Appl. Electrochem.* **4** (1974) 91.
18. D.R. Gabe and F.C. Walsh, *J. Appl. Electrochem.* **13** (1983) 3.
19. D.R. Gabe, G.D. Wilcox, J. Gonzalez-Garcia and F.C. Walsh, *J. Appl. Electrochem.* **28** (1998) 759.
20. B. Poulson and R. Robinson, *Corros. Sci.* **26** (1986) 265.
21. P. Harriott and R.M. Hamilton, *Chem. Eng. Sci.* **20** (1965) 1073.
22. E. Heitz, Chemo-mechanical effects of flow on corrosion, *in* K.J. Kennelley, R.H. Hausler and D.C. Silverman (Eds), 'Flow-induced Corrosion: Fundamental Studies and Industry Experience' (National Association of Corrosion Engineers, Houston, 1991) pp. 1.1–1.29.
23. F.M. Sparrow and J.L. Gregg, *J. Heat Trans.* **81** (1959) 249.
24. T.H. Chilton and A.P. Colburn, *Ind. Eng. Chem.* **26** (1934) 1183.
25. G. Kear, 'Electrochemical Corrosion of Marine Alloys Under Flowing Conditions', Dissertation (University of Portsmouth, Hampshire, UK, 2001).
26. M. Eisenberg, C.W. Tobias and C.R. Wilke, *Chem. Eng. Prog. Symp. Series* **51** (1954) 1.
27. G. Radford, 'The Marine Corrosion and Electrochemical Characteristics of MARINEL Copper Nickel Alloy', Dissertation (University of Portsmouth, Hampshire, UK, 1998).
28. S.C. Dexter and C. Culberson, *Mater. Perform.* **20** (1980) 16.
29. M. Whitfield and D.R. Turner, Seawater as an electrochemical medium, *in* M. Whitfield and D. Jagner (Eds), 'Marine Electrochemistry, a Practical Introduction' (John Wiley & Sons, Chichester, 1981) pp. 3–66.
30. K. Grasshoff, M. Ehrhardt and K. Kremling, 'Methods of Seawater Analysis' (Verlag Chemie, New York, 1983).
31. J.P. Riley and G. Skirrow, 'Chemical Oceanography' (Academic Press Inc., London, 1975).
32. T.R.S. Wilson, Conductometry, *in* M. Whitfield and D. Jagner (Eds), 'Marine Electrochemistry, a Practical Introduction' (John Wiley & Sons, Chichester, 1981) pp. 145–261.
33. G.A. Truesdale, A.L. Downing and G.F. Lowden, *J. Appl. Chem.* **5** (1955) 53.
34. J.S. Newman, 'Electrochemical Systems' (Prentice-Hall Inc., Englewood Cliffs, NJ, 1973).
35. A. Arevalo and G. Pastor, *Anales Quimica* **89** (1993) 497.
36. R. Greef, R. Peat, L.M. Peter, D. Pletcher and M.J. Robinson, 'Instrumental Methods in Electrochemistry' (Ellis Horwood Ltd., Chichester, 1985).
37. R.J.K. Wood, S.P. Hutton and D.J. Schiffrin, *Corros. Sci.* **30** (1990) 1177.
38. F. King, M.J. Quin and C.D. Litke, *J. Electroanal. Chem.* **385** (1995) 45.
39. F.B. Mansfeld, G. Liu, H. Xiao, C.H. Tsai and B.J. Little, *Corros. Sci.* **36** (1994) 2063.
40. R.J.K. Wood and S.A. Fry, *J. Fluids Eng. – Trans.* **112** (1990) 218.
41. F.B. Mansfeld and B.J. Little, *Electrochim. Acta* **37** (1992) 2291.